Mathematical Biosciences 255 (2014) 71–82

Contents lists available at ScienceDirect

Mathematical Biosciences

journal homepage: www.elsevier.com/locate/mbs

Central regulation of heart rate and the appearance of respiratory sinus arrhythmia: New insights from mathematical modeling

Alona Ben-Tal [a,*,1], Sophie S. Shamailov [a], Julian F.R. Paton [b]

[a] Institute of Natural and Mathematical Sciences, Massey University, Albany, Private Bag 102-904, North Shore Mail Centre, Auckland, New Zealand
[b] The School of Physiology and Pharmacology, Bristol CardioVascular, Medical Sciences Building, University of Bristol, Bristol BS8 1TD, UK

ARTICLE INFO

Article history:
Received 19 April 2013
Received in revised form 9 June 2014
Accepted 26 June 2014
Available online 6 July 2014

Keywords:
Mathematical model
Respiratory sinus arrhythmia
Heart rate
Autonomic control

ABSTRACT

A minimal model for the neural control of heart rate (HR) has been developed with the aim of better understanding respiratory sinus arrhythmia (RSA) – a modulation of HR at the frequency of breathing. This model consists of two differential equations and is integrated into a previously-published model of gas exchange. The heart period is assumed to be affected primarily by the parasympathetic signal, with the sympathetic signal taken as a parameter in the model. We include the baroreflex, mechanical stretch-receptor feedback from the lungs, and central modulation of the cardiac vagal tone by the respiratory drive. Our model mimics a range of experimental observations and provides several new insights. Most notably, the model mimics the growth in the amplitude of RSA with decreasing respiratory frequency up to 7 breaths per minute (for humans). Our model then mimics the decrease in the amplitude of RSA at frequencies below 7 breaths per minute and predicts that this decrease is due to the baroreflex (we show this both numerically and analytically with a linear baroreflex). Another new prediction of the model is that the gating of the baroreflex leads to the dependency of RSA on mean vagal tone. The new model was also used to test two previously-suggested hypotheses regarding the physiological function of RSA and supports the hypothesis that RSA minimizes the work done by the heart while maintaining physiological levels of arterial CO_2. These and other new insights the model provides extend our understanding of the integrative nature of vagal control of the heart.

1. Introduction

An optimally-functioning heart is of primary importance to the well-being of the entire organism, so perhaps it is not surprising that heart rate (HR) is tightly controlled by several mechanisms [1]. Factors influencing HR are generally well understood [2] but many questions still remain unanswered. In particular, we are interested in the mechanisms that give rise to respiratory sinus arrhythmia (RSA) – a heart rate variability at the frequency of breathing [3,4] (see Fig. 6). It is widely accepted that the loss of RSA is a prognostic indicator for cardiovascular disease and that the prominent presence of RSA indicates a healthy cardiac system [5], yet the reasons for this are still being debated [6–10].

One controversy is over the main mechanism that gives rise to RSA. Most investigators (for example [6,8]) agree that RSA is mainly due to direct central respiratory modulation of the parasympathetic cardiac signal. Recordings from cardiac vagal motoneurones in the nucleus ambiguus, located in the ventrolateral medulla oblongata, demonstrated waves of excitatory post-synaptic potentials occurring during early expiration [11]. This evidence supports the idea that these neurones are synaptically driven by post-inspiratory respiratory neurones residing within the ventral respiratory column, which is located adjacent to the nucleus ambiguus and thus forming part of a centrally integrated cardio-respiratory network [12]. However, others (for example [7,9]) argue that RSA is mediated by the baroreflex responding to blood pressure oscillations triggered by the abdominal thoracic pump.

Another controversy is over the physiological function of RSA. Hayano et al. [13] hypothesized that the physiological function of RSA is to match ventilation and perfusion in the lungs and thus optimize oxygen (O_2) uptake and carbon dioxide (CO_2) removal. Recently, using mathematical models, we showed that RSA may serve to minimize the energy expenditure of the heart while keeping arterial CO_2 levels at physiological tensions [14]; our theoretical study did not support Hayano's hypothesis.

The models we used in [14] did not include feedback mechanisms of the cardio-respiratory system and numerical simulations were performed by pre-setting the heart rate variations. In this paper we present a model that takes the main features of autonomic heart rate control into account, resulting in the natural

* Corresponding author.
E-mail address: a.ben-tal@massey.ac.nz (A. Ben-Tal).
[1] Equal first place with Sophie Shamailov.

http://dx.doi.org/10.1016/j.mbs.2014.06.015
0025-5564/

appearance of RSA. Our model takes direct central respiratory modulation of the parasympathetic cardiac signal as the main mechanism for RSA but includes blood pressure control via the baroreflex, which allows us to study its effect on RSA.

Many mathematical models that include at least some of the factors that influence the HR have been developed at varying degrees of complexity and emphasis. Some models focus on the calculation of HR given certain parasympathetic and sympathetic signals, but do not include the mechanisms that control the autonomic signals themselves [15–21]. Other models include the baroreflex [22–26] as well as respiratory modulation of the HR either via the central nervous system mechanisms [23,25,26] or via blood pressure which affects the baroreflex [24]. More detailed models take into account several feedback signals that affect cardiac vagal tone such as the baroreflex and pulmonary stretch receptor feedback [27–29] as well as the chemoreflex [28,29] and central respiratory modulation [29]. These more detailed models were used to study a range of phenomena such as HR variability [27], the Valsalva maneuver [29,30], whole-body gas exchange [28] and sleep apnea [29] but did not investigate the controversies surrounding RSA described above.

Several studies aiming at modeling RSA specifically have been published. Barbi et al. [31] developed an integrate-and-fire model with an oscillating threshold that mimics RSA. Other models described the relationship between respiration and heart rate using transfer functions [32,33] or treated the lungs and the heart as two coupled oscillators (see, e.g., [34,35]). These models were used to mimic RSA [32], study the heart rate transient during inspiration or expiration [33] and show that the respiratory system can affect heart rate [34]. A Hodgkin–Huxley type model of the sinus node was developed in [36] and used to study the time-course of RSA when the vagal activity oscillated at the frequency of breathing. Negoescu and Csiki [37] developed a model partly based on [16] that takes into account respiratory effects on HR via the parasympathetic system, but also includes the sympathetic influence on the heart. They compared the output of their model to several experiments related to RSA, most notably the dependence of RSA on breathing frequency and on vagal tone.

The model we present in this paper is different from all previously-published models described above. It includes physiological features not previously included in RSA-specific models (such as respiratory gating of the baroreflex [38,39]) and omits other features that have been taken into account in other, more detailed models (such as the chemoreflex, which we think is less important for the purpose of studying RSA). The model is relatively simple compared to some of the previously-published models but we show that it can still reproduce a wide range of physiological observations and that it can be used to study the causes and benefits of RSA, as well as making novel predictions.

2. Methods

Our study consists of three sections: model development (Section 3), parameter fitting (Section 4.1) and model testing (Section 4.2). Throughout the paper we compare our model simulations with a range of published experimental data, summarized in Table 1. One set of experiments is used to set parameters (this is indicated by a star in Table 1) and another to test the model. The ENGAUGE software available from [40] was used to extract experimental data from published figures. In addition we used mathematical analysis and time simulations to explain the model output, produce new predictions and re-examine the two hypotheses regarding the physiological function of RSA. RSA can be observed in both the heart rate (HR) and the heart-beat period (T_L) and both quantities are used in the experimental literature.

Table 1
Main experiments used for comparison with model output. T_L stands for heart beat period, MAP for mean arterial pressure, RSA for respiratory sinus arrhythmia, SA for sinoatrial and f_R for respiratory frequency. The star indicates experiments that were used to set parameters.

Experiments	References	Species
Dependence of T_L on MAP*	[41–45]	humans
Dependence of RSA on vagal tone*	[46,47] [48]	Dogs Humans
Dependence of RSA on lung volume*	[49–53]	Humans
Dependence of RSA on breathing frequency*	[54] [32,55–57]	Cats Humans
Time response of the SA node	[17,58]	Dogs
Dependence of phase between RSA and lung volume on f_R	[54] [32,57,59]	Cats Humans

Note that some experimental studies derive these quantities directly from recorded time series of HR or T_L while some first perform a Fourier transform. Often in the latter case RSA amplitude refers to the spectral power of the peak in the Fourier transform at breathing frequency. However, whenever possible, we compare our model output to the same exact quantity in the experiments. In the rest of the paper, as in the experimental literature, RSA amplitude, magnitude and strength are used interchangeably and refer to the amplitude of oscillations in T_L and in HR (note however that $HR = 1/T_L$).

3. Model assumptions and description

For convenience, we list all the variables and parameters that are introduced in this section and their physiological meaning in Table 2.

The heart, if denervated, will beat at its intrinsic rate (set by the pacemaker cells in the sinoatrial node) of about 100 beats per minute (bpm). However, the two limbs of the autonomic nervous system constantly innervate the heart: the sympathetic system acts to accelerate the HR while the parasympathetic (acting through the cardiac vagal nerve) decelerates it [60]. The rate of change of the heart-beat period can thus be modeled by:

$$\frac{d\,T_L}{d\,t} = -S_1(T_L - T_{L0}) + c_0 C_{VN} - S_M, \tag{1}$$

where T_L is the heart-beat period (R–R interval), T_{L0} is the intrinsic period of the heart, C_{VN} is the integrated cardiac vagal signal (also referred to as *vagal tone*), S_M represents the sympathetic drive to the heart and S_1 and c_0 are constants. It is well-known that the sympathetic system acts on a much slower time-scale than the parasympathetic [17]. Therefore, we take S_M as being constant in time while C_{VN} is a dynamic variable. We take into account three main factors that affect the vagal tone:

- The baroreflex strives to keep blood pressure constant [61], and since mean arterial pressure (MAP) is proportional to HR, if MAP changes, the arterial baroreceptors send a signal to the heart (via the autonomic nerves) to change HR accordingly. In addition, experiments show that the baroreflex signal is only effective during expiration although the exact location of this gating by respiration is unknown [62–66].

Table 2
Glossary defining all the variables and parameters used in the heart rate control model. Table 4 defines the variables of the lung model.

Symbol	Meaning	Units
HR	Heart rate	Hz
T_L	Heart beat period	s
T_{L0}	Intrinsic heart beat period of the Sinoatrial node (constant)	s
C_{VN}	Integrated cardiac vagal nerve signal	–
C_{VN0}	Unmodulated central parasympathetic Vagal activity (constant)	–
S_M	Integrated cardiac sympathetic signal (constant)	–
S_1, S_2	Response frequencies of T_L and C_{VN}, respectively (constants)	Hz
c_{0-3}	Constants affecting the strength of:	
c_0	– Parasympathetic input to the heart	–
c_1	– Central respiratory signal	Hz
c_2	– Mechanical feedback from the lungs	$(\text{s L})^{-1}$
c_3	– Baroreflex input to the heart	Hz
k_2	Constant affecting the mechanical Feedback from the lungs	L
G	Central-respiratory baroreflex gating function	–
a	Constant affecting the slope of the gating function	s/L
B_R	Baroreflex input to cardiac vagal tone	–
R_s	Systemic resistance (constant)	mmHg s/L
V_c	Stroke volume (constant)	L
δ	Ideal mean arterial pressure (constant)	mmHg
γ	Constant affecting the strength of the baroreflex	mmHg^{-1}
k_3	Constant affecting the baroreceptor signal	–
MAP	Mean arterial pressure	mmHg
A	Central respiratory rhythm-generating signal	–
R_p	Phrenic nerve signal	–
q	Airflow into the lungs	L/s
V_A	Lung volume	L

- The central respiratory signal generated in the brainstem (which drives the lungs) modulates the parasympathetic tone directly [11,12,67].
- Mechanical stretch receptors located on terminal bronchioles in the lungs detect the instantaneous alveolar inflation volume. The signal from these stretch receptors inhibits the cardiac vagal signal [46] but the exact neural pathway by which this occurs is still unknown.

A schematic description of all of these physiological factors is shown in Fig. 1.

The equation for the rate of change of the integrated cardiac vagal signal is given by:

$$\frac{d\,C_{VN}}{d\,t} = -S_2(C_{VN} - C_{VN0}) - c_1 A + c_2(k_2 - V_A) + c_3 G(qA) B_R(T_L), \quad (2)$$

where C_{VN0} is the central parasympathetic vagal activity in the absence of any other inputs, A is the central respiratory rhythm-generating signal (modeled as a square wave; see Fig. 1(a)) and V_A is the instantaneous lung volume. $G(qA)$ is a gating function that depends on both A and the pulmonary air-flow, q. $B_R(T_L)$ is the input from the baroreceptors (note that MAP=$V_c R_s/T_L$ and hence depends on T_L, see more details below) and S_2, c_1, c_2, c_3 and k_2 are constants (see Section 4.1 and Table 3 for more details). G is given by:

$$G(qA) = \frac{1}{1 + e^{a(qA)}}. \quad (3)$$

where a is a constant. A plot of this function with default parameters (see Table 3) is shown in Fig. 1(h).

B_R, the baroreflex term, can be taken as one of the following (see also Fig. 1(f)):

- the full sigmoidal curve (functional form as in, e.g., [61])

$$B_R(T_L) = \frac{1}{1 + \exp\left\{\gamma\left(\frac{V_c R_s}{T_L} - \delta\right)\right\}} - k_3, \quad (4)$$

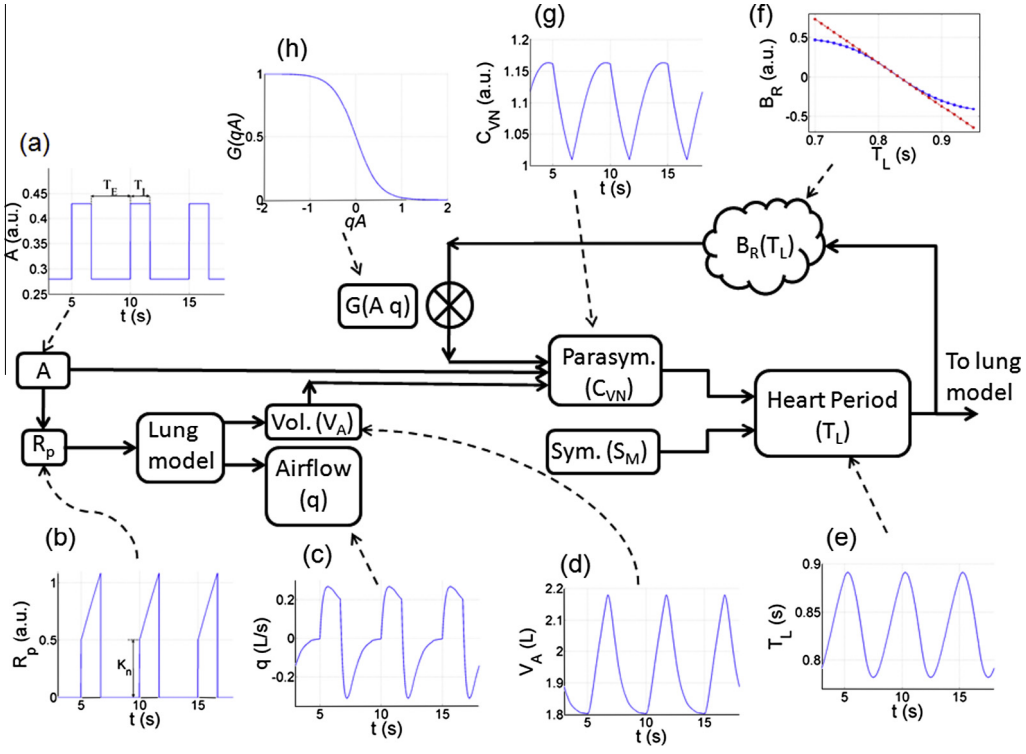

Fig. 1. A schematic description of the heart rate control model for mammals. (a) Central rhythm-generating signal A, (b) phrenic nerve signal R_p, (c) airflow q, (d) lung volume V_A, (e) heart beat period T_L, (f) afferents from the baroreceptors, $B_R(T_L)$ (showing the linearized and full, non-linear versions), (g) integrated cardiac vagal signal C_{VN}, and (h) respiratory gating function $G(Aq)$. Time-series results produced with the linear baroreflex. The lung model is described in Appendix A.

Table 3
Default parameters for the model of heart rate control for humans. When units are not shown, the parameters are dimensionless. All parameter-fittings were done with the linear baroreflex. c_3, γ and R_s were found using Levenberg–Marquardt non-linear regression. In all other cases, fitting a parameter implies that the parameter was varied until the model output matched the experimental value to one or two significant figures.

Parameter	Value	Justification
S_1	0.435 Hz	Fits the peak frequency in Fig. 5 (linear B_R)
T_{L0}	0.6 s	Gives an intrinsic HR of 100 bpm
c_0	1	Arbitrary; setting to zero mimics vagotomy
S_M	1	Ensures $C_{VN} > 0$ for physiological conditions
S_2	0.435 Hz	Assumed to be the same as S_1
C_{VN0}	1.484	Gives HR of 72 bpm under normal conditions
c_1	0.85 Hz	Fits RSA peak amplitude in Fig. 5 (linear B_R)
c_2	0.05 (s L)$^{-1}$	Fits gradient in Fig. 4.
k_2	4.2 L	Gives 15 bpm increase in HR if c_2 is set to 0
c_3	0.21 Hz	c_3, γ and R_s were fitted to data in Fig. 2
γ	−0.1945 mmHg^{-1}	–
R_s	1119 mmHg s/L	Value is in the physiological range [60]
δ	94 mmHg	Normal MAP in humans [60]
V_c	0.07 L	Averaged stroke volume in humans [2,69]
k_3	0.5	Ensures $B_R = 0$ when MAP is normal
a	4 s/L	Gives the linearized slope of G around 0

- the linearized version (found by linearizing Eq. 4 around $T_L = V_c R_s/\delta$)

$$B_R(T_L) = \frac{\gamma\delta^2}{4}\left[\frac{T_L}{V_c R_s} - \frac{1}{\delta}\right], \tag{5}$$

where V_c is the stroke volume, R_s is the systemic vascular resistance, δ is the ideal MAP and k_3 and γ are constants (see Table 3 for more details). Although the non-linear version is a much better description of reality, the linearized function will prove to better reproduce experimental results for reasons discussed in Section 5.1. Note that $\text{MAP} = V_c R_s \text{HR} = V_c R_s/T_L$ and that V_c and R_s are constants in our model.

The two differential Eqs. (1) and (2) are coupled to a model of the lungs (also referred to in Fig. 1) which is based on [68] and is described for convenience in Appendix A. The differential equations of the lung and heart-rate models are solved together: lung volume from the lung model acts as input to the heart rate model and the heart beat period from the heart rate model serves as input in the lung model. An important point to note is that respiration is in open-loop; we are thus able to choose the respiratory period, T_R, set the relative duration of T_I and T_E (inspiratory and expiratory times), and control the amplitude of respiration via the parameter K_n (see Fig. 1(a) and (b)). This enables us to mimic experiments where subjects are told to breathe in a particular way. Another point to note is that the lung model uses a discrete heart rate to calculate blood gas tensions (which are included in the model but not used for heart rate or ventilation control in the present study). Discrete heart beat times are obtained in the following way: the quantity $2\pi/T_L$ is integrated over time and whenever it crosses a multiple of 2π, a heart-beat occurs.

4. Results

We used a wide range of numerical experiments to set the parameters of our model, test the model and make new testable predictions. Table 1 summarizes the main published experimental data with which we compared the model simulations. This section gives a detailed description of all the numerical experiments we did. For clarity, the result section is divided into two parts. In Part A, we describe all the numerical experiments we used to set the parameters of our model and in Part B we describe all the numerical experiments we used (or that could in principle be used) to test the model. As will be seen, both subsections provide new insights on the physiology.

4.1. Results: Part A – Setting the parameters

The results in this subsection were obtained while fitting parameters to the heart control model. We show that by choosing the parameters as described in Table 3, the model can reproduce several experiments, substantiating its validity (Figs. 2–5). We also provide novel explanations for some of the experimental observations.

4.1.1. Dependence of heart-beat period on mean arterial pressure

Fig. 2 shows the baroreflex response curve. The top panel summarizes several published results from the literature (measurements performed on humans). A large variation becomes immediately apparent – partly, this is due to the technique used. The shallowest curves (red squares [41] and dark green triangles [42]) have employed neck suction to alter MAP, and this only activates the carotid baroreceptors. The steepest curves (purple stars [45] and teal diamonds [44]) used vasoactive agents to change blood pressure directly, thus activating the aortic baroreceptors also. The solid blue line with circles is the theoretical curve from [43] (based on a few experimental data points using neck suction [70]). All these curves were shifted to a common mid-point – both vertically and horizontally. A vertical shift corresponds to a different ideal mean heart rate, and horizontal shifts were mostly necessary because some authors plot systolic pressure versus T_L, not MAP. We chose to adopt the curve from [43] (blue line with circles) because it lies between the results of [41,44]. Moreover, [44] gives six data sets for people in different age groups, some of whom were inevitably hypertensive. The teal curve with diamonds reproduced here is the healthiest, youngest group, but an average person would probably have a response curve closer to the dark blue line with circles. Later on, in Section 5, we consider the effect of changing the slope of the baroreflex response.

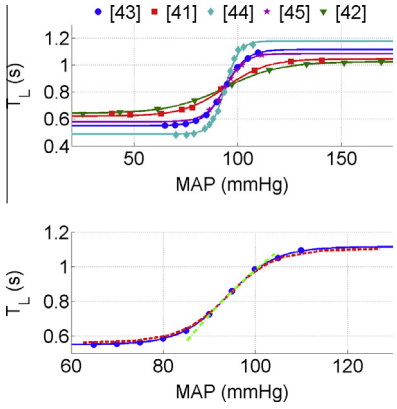

Fig. 2. Heart beat period (T_L) as a function of mean arterial pressure (MAP). Upper panel: A selection of cardiac baroreflex response curves from the literature, some using neck suction [41,43,42] and some injections of vasoactive agents [44,45] to change blood pressure. All data sets were shifted to a common mid-point. Lower panel: Blue line with circles is the theoretical curve from [43] based on experimental results from [70], dashed red line is calculated with the model using the nonlinear B_R, while the dash-dotted green line uses the linear B_R. For model simulations, we had $T_I = 0.5T_E$, c_1 and c_2 were set to zero (no RSA) and $C_{VN0} = 1.101$ was chosen so that mean HR was 72 bpm. MAP was changed by varying R_s, the systemic resistance. (For interpretation of the references to color in this figure legend, the reader is referred to the web version of this article.)

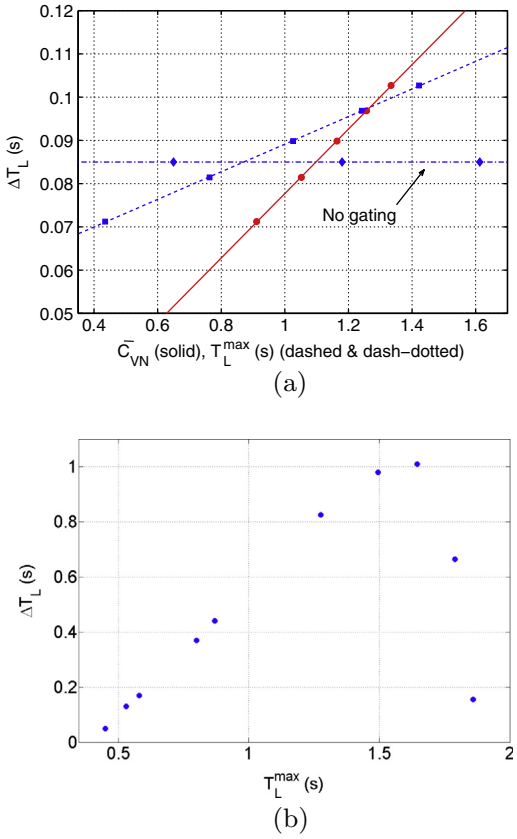

Fig. 3. The magnitude of RSA increases linearly with mean vagal tone (average of C_{VN} over one breathing period), as found experimentally. (a) Model results with linear B_R as we change MAP. This is done by setting MAP=$V_c R_s/T_L$ in the expression for B_R to given values. Otherwise, $2T_I = T_E$ and default parameters are used. The blue lines (dashed and dash-dotted) correspond to x-axis units of T_L^{max} (the longest heart-beat period attained during a breath) and the solid red line corresponds to x-axis units of mean vagal tone, $\bar{C}_{VN}$. The flat line shows the response when $G(qA) = 1$ (i.e. when there is no gating, see Eq. (2)). (b) Data extracted from Fig. 3 of [46]. Note that T_L^{max} is proportional to mean C_{VN} and mean T_L as MAP is changed. (For interpretation of the references to color in this figure legend, the reader is referred to the web version of this article.)

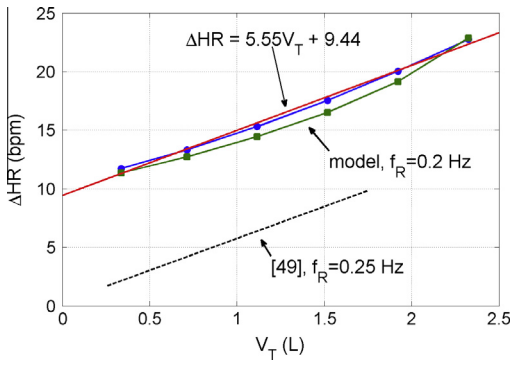

Fig. 4. Roughly linear dependence of RSA amplitude on tidal volume (V_T) agrees with experiments. $T_I = T_E$ with default parameters. Linear B_R in blue circles, nonlinear B_R in green squares. The red solid line is a least-squares fit to the model output with linear baroreflex. The black dashed line is a least-squares fit to experimental data from [49]. (For interpretation of the references to color in this figure legend, the reader is referred to the web version of this article.)

In the bottom panel of Fig. 2, we reproduce the data from [43] (blue line with circles). The dashed red line shows the model calculation using the nonlinear B_R, and the dash-dotted green line shows the model calculation using the linear B_R. These model results were

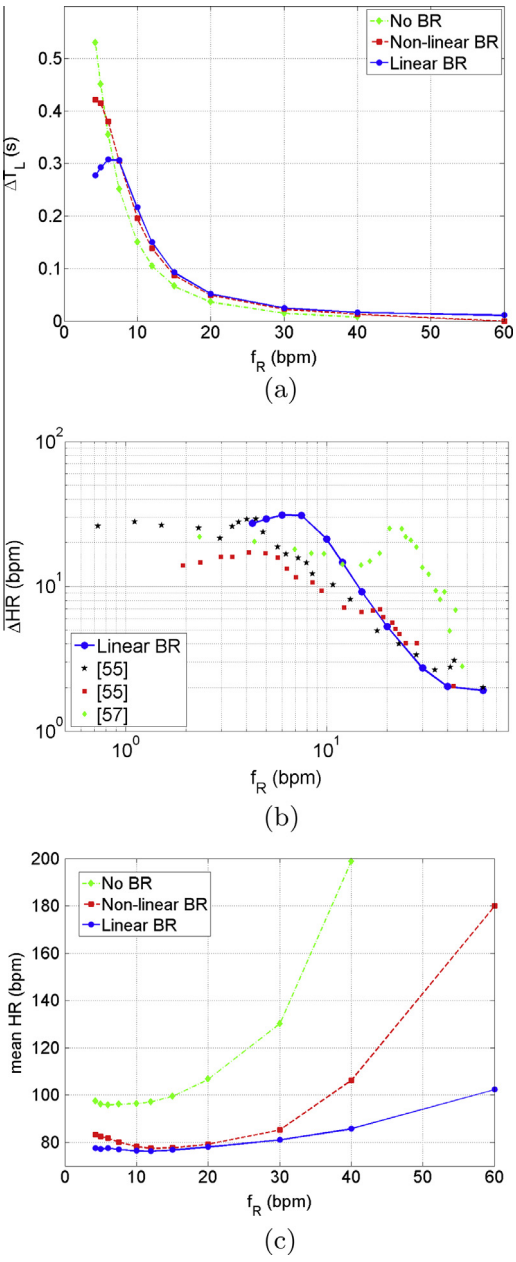

Fig. 5. RSA amplitude peaks at a small respiratory frequency. (a) ΔT_L as a function of respiratory frequency (f_R in breaths per minute, bpm). (b) Experimental data compared with one curve from (a) on a log–log plot. (c) Mean HR as a function of respiratory frequency. V_T = 1 L for all points and $T_I = T_E$. Solid blue lines – default cardiac parameters with the linear baroreflex. Dashed red lines – default cardiac parameters with the non-linear baroreflex. Dash-dotted green lines – the baroreflex has been removed by setting $c_3 = 0$. (For interpretation of the references to color in this figure legend, the reader is referred to the web version of this article.)

obtained without respiratory modulation ($c_1 = c_2 = 0$) which required setting $C_{VN0} = 1.101$ so that mean HR was still 72 bpm under normal conditions. MAP $= \frac{V_c R_s}{T_L}$ was changed by varying R_s, the systemic resistance. T_L was recorded once the system reached steady state. As can be seen in Fig. 2, our model captures the dependence of mean heart-beat period on MAP well. In the central region, close to MAP of 94 mm Hg, the baroreflex curve is well approximated by the linear B_R option.

4.1.2. Dependence of RSA on vagal tone

It has been observed experimentally that when mean HR is changed by stimulating the carotid baroreceptors, the amplitude

of RSA changes linearly with the mean cardiac vagal tone (the average of C_{VN} over a breathing period) [47,48,46]. Fig. 3(a) shows that our model can reproduce this linear relationship. In red (solid line), we plot RSA against mean vagal tone, and in blue (dashed and dash-dotted lines) we show RSA versus maximum heart period, T_L^{max}. T_L^{max} is the longest heart-beat period attained during a breath and is proportional to mean C_{VN}. Fig. 3(b) shows data extracted from Fig. 3 of [46]. We found that this linear dependence is due to the gating of the baroreflex signal (compare the dashed and dash-dotted lines in Fig. 3(a)). Without the gating, the mean cardiac vagal tone would change as MAP changes but the amplitude of its oscillations would remain unaltered and hence there would be no change in the amplitude of RSA (i.e. ΔT_L would not be affected). The amplitude of RSA in Fig. 3(b) is an order of magnitude larger than in our results probably because [46] performed the experiments on dogs which have a much shorter natural cardiac period than humans (so a larger C_{VN} is needed to bring it to the same range of values as that in Fig. 3). Ref. [48] presents figures which have heart-period variations of the same order of magnitude as our model generates[2]. The model results are practically unchanged if one uses the non-linear baroreflex instead or if a, the slope of $G(qA)$, the gating function (see Eq. (3)) changes between $a = 3.5$ and 4.5. Note that we do not include the abrupt drop in RSA as heart period reaches 1.7 s (see Fig. 3(b)). This omission will not affect the simulations if HR does not drop below 35 bpm.

4.1.3. Dependence of RSA on lung volume

The dependence of RSA on tidal volume is shown in Fig. 4. The model output (at breathing frequency of 0.2 Hz) with linear baroreflex is shown in blue (circles) and the model output with nonlinear baroreflex is shown in green (squares). A least-squares fit to the model output with the linear baroreflex is shown in red (solid line) and gives a slope of 5.55 bpm/L. This agrees with [49] which found the relationship between ΔHR and V_T to be linear with a gradient of 5.45 bpm/L at a breathing frequency of 0.25 Hz (see the black dashed line in Fig. 4) and with a gradient of 6.23 bpm/L at a breathing frequency of 0.1 Hz (not shown in Fig. 4). As can be seen in Fig. 4, the red solid line (the least-squares fit to the model output) lies above the experimental data (that is, the y-intercept of the red line is shifted upwards). This is to ensure that when $V_T = 0.5$ L, $\Delta\text{HR} \approx 12$ bpm which is more realistic than the value found in [49].

4.1.4. Dependence of RSA on respiratory frequency

Fig. 5(a) show the dependence of RSA amplitude on respiration frequency (f_R) when tidal volume is kept constant. The solid blue curve shows model results with linear B_R and default parameters. The dashed red curve shows model results with the nonlinear B_R and the dash–dotted green curve shows model results when the baroreflex has been removed (by setting $c_3 = 0$). RSA behaves as expected from the literature [54,32,55–57] when the linear B_R is used. Data from some of these experiments in humans is shown in panel (b) alongside one of our model results. Note that all the experimental data exhibit a maximum value as predicted by our model and that the parameters we have chosen for our model is within the physiological range. In particular, the corner frequency at which RSA amplitude peaks (Fig. 5(a)) is 6–7 bpm and the maximal RSA magnitude reached during slow breathing is about 30 bpm – both agree with experimental data (e.g. see [55,32,57]). The gradient of the fall-off is within the physiological range. Fig. 5(c) shows the dependency of mean HR on respiratory frequency. For higher frequencies there is a rise in mean HR which is steeper when the nonlinear B_R is used and steeper still when there is no baroreflex.

The strong influence of the baroreflex on the peak seen in Fig. 5(a) when the linear baroreflex is used can be explained with the help of a simplified version of the differential equations for C_{VN} and T_L. Consider the following system:

$$\frac{dx}{dt} = -S_1(x - x_0) + b_1 y, \tag{6}$$

$$\frac{dy}{dt} = -S_2(y - y_0) - b_2 x - d\sin(\omega t). \tag{7}$$

where $x = T_L, y = C_{VN}, x_0 = T_{L0} - S_M/S_1, b_1 = c_0, y_0 = C_{VN0} + c_2 k_2/S_2 - c_3\gamma\delta/(4S_2)$ and $b_2 = -c_3\gamma\delta^2/(4V_c R_s)$. (Note that $\gamma < 0$ and $b_2 > 0$). The sinusoidal term represents the simplest form of modulation of the vagal signal (representing both the central and peripheral respiratory drive). The baroreflex is taken as linear, and no respiratory gating of B_R is included.

We are interested in the long-term solution of $x(t)$. This system can be solved analytically and the solution for x has the form

$$x(t) = \zeta + \Omega\sin(\omega t + \varphi), \tag{8}$$

where ζ, Ω, ω and φ are constants. In particular, we want to investigate the dependence of Ω (corresponding to RSA amplitude) on the different parameters. We have

$$\Omega = \frac{db_1}{\sqrt{\left(S_1^2 + S_2^2 - 2b_1b_2\right)\omega^2 + (S_1S_2 + b_1b_2)^2 + \omega^4}}. \tag{9}$$

It can be shown that Ω has two extrema: one at $\omega_1 = 0$ and another at

$$\omega_2 = \sqrt{b_1b_2 - 0.5(S_1^2 + S_2^2)}. \tag{10}$$

If $b_1b_2 - 0.5(S_1^2 + S_2^2) > 0, \omega_1$ is a minimum and $\omega_2 \in \mathbb{R}$ is a maximum. If, on the other hand, $b_1b_2 - 0.5(S_1^2 + S_2^2) < 0$, ω_2 becomes pure imaginary and we have only one extremum at $\omega_1 = 0$, which is now a maximum. This latter case will certainly apply when $b_2 = 0$ (no baroreflex) and explains why without the baroreflex we see no reduction in RSA magnitude when the frequency of breathing is reduced below ω_2. This observation could also be explained as follows: at low respiratory frequencies the barorereflex has more time to bring the oscillating heart rate back to its desired value, leading to a reduction in RSA amplitude. The HR can no longer be controlled without the baroreflex or when the nonlinear B_R saturates (which is what happens at low respiratory frequencies in our model) and the reduction in RSA amplitude disappears.

Eq. (10) shows the connection between the peak frequency ω_2, the strength of the baroreflex b_2 and the response frequency of the sinoatrial node $S_1 = S_2 = S$. We can use this fact to set parameters in our model and check the sensitivity of the results to changes in parameters. For example, if we fix the peak frequency ω_2 (the value is known from experiments) and calculate the effective b_2 value based on the curves in Fig. 2 we can then calculate the corresponding value of S (assuming $b_1 = 1$). Increasing b_2 by a factor of 1.84 (to match the teal curve with diamonds of Fig. 2) increases S by a factor of 1.38, and decreasing b_2 by a factor of 3 (to match the red curve with squares of Fig. 2) decreases S by a factor of 1.85 (recall that the default values were based on the blue curve with circles in Fig. 2). An increase in S will lead to a faster response to direct stimulation of the sinoatrial node (see Section 4.2.2) but will not change the results in this section qualitatively. Note that since $b_2 = -c_3\gamma\delta^2/(4V_cR_s)$, a wide range of possible changes in the model parameters will affect the results in a similar way. Changing c_1 moves the peak in Fig. 5 up and down. Taking

[2] We did not compare our model to [48] directly because there, in contrast to [46], the mean heart rate was changed by varying respiratory period which is known to affect RSA as well as mean HR.

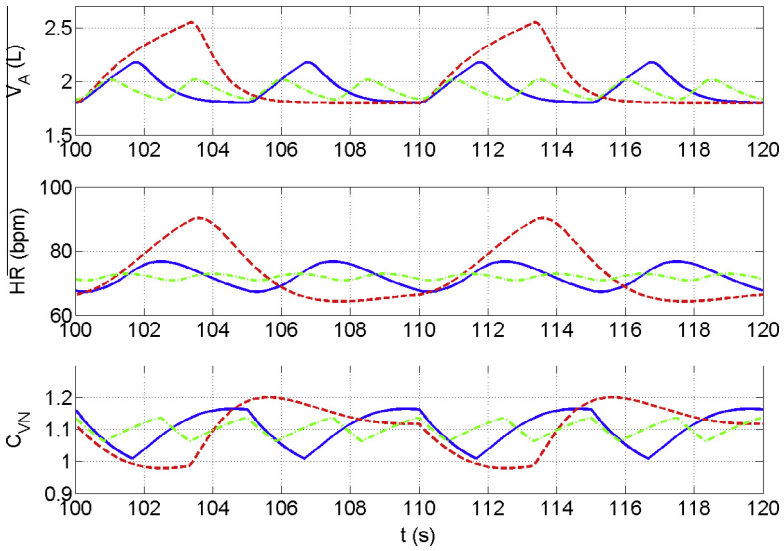

Fig. 6. RSA amplitude is largest under deep, slow breathing, as found experimentally. Linear B_R and $2T_I = T_E$ are used for all simulations. Minute ventilation was kept the same in all cases. Solid blue lines: T_R = 5 s, V_T = 0.3768 L (K_n = 0.5). Dashed red lines: T_R = 10 s, V_T = 0.7552 L (K_n = 0.74). Dash-dotted green lines: T_R = 2.5 s, V_T = 0.1879 L (K_n = 0.562). Panels from top down: lung volume (V_A), heart rate (HR) and integrated vagal nerve activity (C_{VN}). (For interpretation of the references to color in this figure legend, the reader is referred to the web version of this article.)

$c_1 = 0.7$ Hz (compared to the default 0.85 Hz) reduces the peak RSA to 20.8 bpm (compared to 30 bpm with default parameters). Increasing c_1 to 1 Hz causes the peak RSA to go up to 46 bpm. However, this will not affect the results in this section qualitatively.

4.2. Results: Part B – Testing the model

All the results presented in the previous subsection have been used to set the model parameters (see Table 3). We now present other results and new predictions based on these model parameters and equations.

4.2.1. Appearance of RSA

Fig. 6 shows $V_A(t)$, HR(t) and $C_{VN}(t)$ as calculated by the model (using linear baroreflex and default parameters) for different respiratory patterns, keeping minute ventilation constant (minute ventilation is the total volume of air inhaled in a minute). We see that deep, slow breathing increases RSA amplitude while shallow and fast breathing diminishes it. This observation is not altered by the use of the non-linear B_R.

4.2.2. Time response of the sinoatrial node

We can mimic direct stimulation of the sinoatrial node with our model. First, RSA and the baroreflex are turned off ($c_{1,2,3} = 0$) and the tonic parasympathetic signal, C_{VN0} is adjusted such that HR = 72 bpm. Then a step change in C_{VN0} is induced. The response time of about 15 s seen in our model is of the same order of magnitude as found experimentally in dogs[3] [17,58] even though S_1 and S_2, which influence the sinoatrial node time response, were chosen to fit the corner frequency in Fig. 5. Note that Eq. (10) reveals that there is a link between the slope of $B_R(T_L)$ and the parameters S_1 and S_2. Had we used the teal curve with diamonds in Fig. 2, where the slope is steeper but kept the corner frequency in Fig. 5 the same, then the response time would have been faster (about 10 s, same as [17,58]).

[3] In these invasive animal experiments, the vagal and sympathetic cardiac nerves were exposed and stimulated directly by a step-function voltage signal.

4.2.3. Phase difference between heart rate and lung volume as a function of breathing frequency

Fig. 7 shows the phase difference between HR and lung volume as a function of respiratory frequency. Several experimental results are available to confirm these findings [32,54,57,59]. Each reference uses a slightly different definition of phase. We define the phase difference to be the phase between a peak in the heart-beat period (T_L) and the preceding trough in the volume. The experimental results themselves show some variability, but our results are qualitatively similar to all the papers cited above. We plot on a logarithmic scale for easier comparison with experiments. Our curves have the same shape as those shown in [54], but the experimental semi-log graph shows a plateau at low frequencies, a region to which our simulations do not extend. The experimental data from [32] and our graphs also have the same shape. Comparing to [57], their high-frequency plateau in the semi-log graph is not as pronounced as in our simulations. Finally, as for [59], for

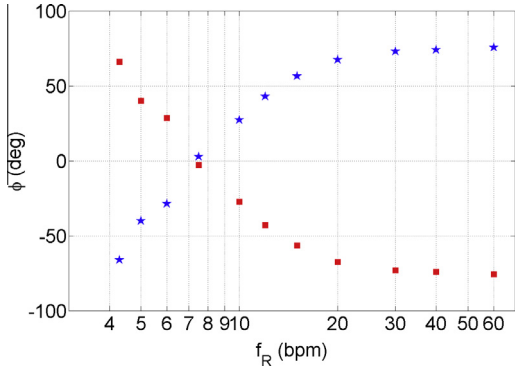

Fig. 7. The phase between heart rate (HR) and lung volume (V_A) is in qualitative agreement with experimental observations. Red squares – the phase difference ($\Delta\phi$) between a peak in the heart period (T_L) and the preceding trough in the lung volume. Blue stars – negative values of red squares for easier comparison with the literature. Simulations performed with the linear $B_R, T_I = T_E$ and $V_T = 1$ L. The model output is plotted on a logarithmic scale for easier comparison with experiments [32,54,57,59]. (For interpretation of the references to color in this figure legend, the reader is referred to the web version of this article.)

the range of frequencies that this reference covers, the shape of the curve is the same as in our model. The results with non-linear baroreflex are qualitatively similar.

4.2.4. Dependence of mean HR on lung volume

Fig. 8 shows the mean heart rate as tidal volume is changed when either the linear or the nonlinear baroreflex function is used. The mean HR is linear in V_T only when the baroreflex function is taken as linear. We were unable to find a similar systematic experimental study in the literature, so the functional dependence of mean HR on tidal volume in Fig. 8 constitutes a prediction for future experimental testing.

4.2.5. Dependence of RSA on mean HR

Fig. 9 shows the HR as a function of time over a single breath with different mean HR values as calculated with the linear baroreflex. The ventilation was kept constant with equal inspiration–expiration times, a 5 s total respiratory period, and a tidal volume of 0.5 L. The mean HR was decreased by increasing the value of C_{VN0} which resulted in a lower averaged blood partial pressure of CO_2 (denoted as $\bar{p}_{ce}$ and calculated by averaging the value of p_c at the end of a heart period, over one breath). In the linearized model, the delay between the end of inspiration and the peak in HR decreases when mean HR increases, while in the non-linear model, the time delay increases when mean HR deviates either way from normal.

4.2.6. Larger inspiration-to-expiration ratio decreases the time between end of inspiration and the peak in HR

Fig. 10, produced with the linear baroreflex, shows how HR is affected by the inspiration-to-expiration ratio. The top panel in Fig. 10(a) shows the airflow into the lungs and the bottom panel shows the heart rate. The horizontal bars show the inspiration period as defined by $A(t)$. Fig. 10(b) shows the time between end of inspiration and the peak in HR as a function of T_I/T_E when $\bar{p}_{ce}$, the averaged blood partial pressure of CO_2, was constrained to 38 mm Hg (blue stars, value is within the normal human range) and when the mean HR was constrained to 67 bpm (red squares, value is within the normal human range). These results are similar to experimental data showing maximal HR occurring during early expiration with the same phase dependence on T_I/T_E (see Fig. 3 of [71]) and are not expected to be altered by the non-linear baroreflex as HR stays close to the ideal, with moderate RSA.

4.2.7. The physiological significance of RSA

As discussed in the Introduction, one of the controversies surrounding RSA is the question of its physiological function. Here we test the two hypotheses previously suggested for the function

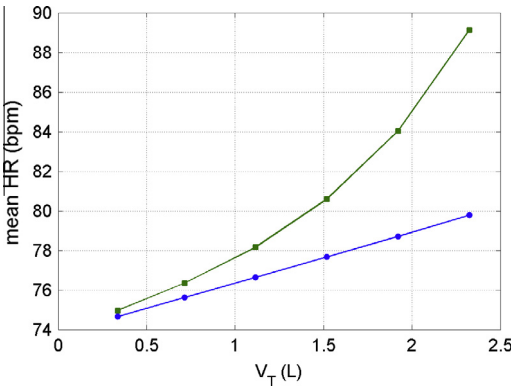

Fig. 8. A prediction for the behavior of mean heart rate as tidal volume is varied. The figure shows mean heart rate (HR) as a function of the tidal volume (V_T). Blue circles – linear B_R, green squares – nonlinear B_R. (For interpretation of the references to color in this figure legend, the reader is referred to the web version of this article.)

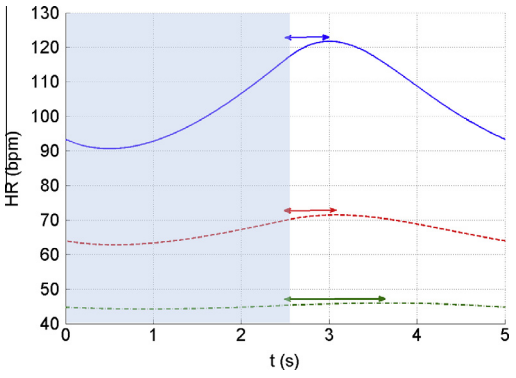

Fig. 9. Lower mean heart rate (HR) reduces RSA amplitude and increases the peak-HR time-delay when the linear baroreflex is used. $V_T = 0.5$ L ($K_n = 0.46$), $T_R = 5$ s, $T_I = T_E$, and the linear version of B_R is used. Solid blue lines: $\bar{p}_{ce} = 39$ mmHg, $C_{VN0} = 1.1$, dashed red lines: $\bar{p}_{ce} = 38$ mmHg, $C_{VN0} = 1.65$, dash-dotted green lines: $\bar{p}_{ce} = 37$ mmHg, $C_{VN0} = 2.4$. Shaded area shows inspiration time. (For interpretation of the references to color in this figure legend, the reader is referred to the web version of this article.)

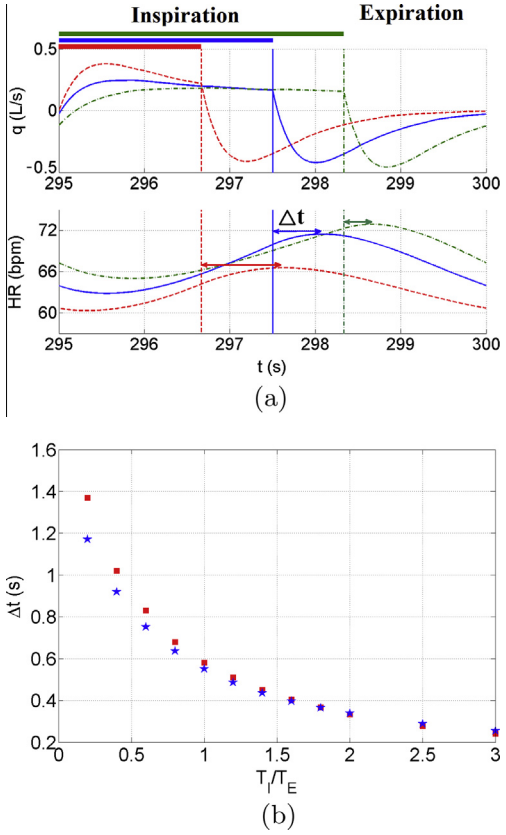

Fig. 10. Larger inspiration-to-expiration ratio (T_I/T_E) decreases the time between end of inspiration and the peak in HR. (a): Top panel shows airflow into the lungs (q) and the bottom shows the heart rate (HR). $T_R = 5$ s and minute ventilation is 5.964 L/min. $\bar{p}_{ce}$ was constrained to 38.00 mmHg for all three curves. Blue solid curves: $T_I/T_E = 1$, $K_n = 0.46$, $C_{VN0} = 1.65$. Red dashed curves: $T_I/T_E = 0.5$, $K_n = 0.805$, $C_{VN0} = 1.68$. Green dash-dotted curves: $T_I/T_E = 2$, $K_n = 0.235$, $C_{VN0} = 1.67$. Horizontal bars show the inspiration period (T_I) as defined by $A(t)$. (b): the time between end of inspiration and the peak in HR as a function of T_I/T_E when $\bar{p}_{ce}$ was constrained to 38.00 mmHg (blue stars) and when the mean HR was constrained to 67 bpm (red squares). (For interpretation of the references to color in this figure legend, the reader is referred to the web version of this article.)

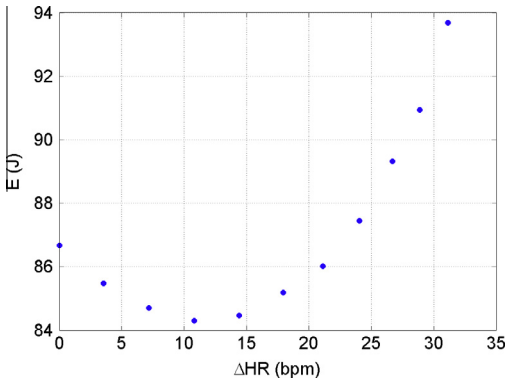

Fig. 11. RSA minimizes the work done by the heart while maintaining arterial CO_2 levels. $T_R = 10$ s, $V_T = 1$ L ($K_n = 0.83$), $T_I = T_E$. c_0 is decreased steadily and S_M is adjusted to keep mean p_{ce} at its initial value of 37.11 ± 0.02 mmHg (when $c_0 = S_M = 1$ with the linear baroreflex). Energy per heart-beat (E) is calculated and plotted as a function of HR variation. Linear baroreflex is used.

Table 4
Summary of parameters of the lung model.

Parameter	Meaning	Units	Value
P_m	Atmospheric pressure	mmHg	760
C_u	Unit conversion factor	L/mol	25.426
T_L	Heart beat period	s	5/6
p_w	Water vapor pressure at 37 °C	mmHg	47
f_{om}	Dry atmospheric O_2 fractional concentration	–	0.21
f_{cm}	Dry atmospheric CO_2 fractional concentration	–	0
V_T	Tidal volume	L	0.4
V_D	Dead-space volume	L	0.15
V_c	Capillary volume/heart stroke volume	L	0.07
R	Airway resistance to flow	mmHg s/L	1
E	Lung elastance	mmHg/L	2.5
T_R	Respiratory period	s	5
f_R	Respiratory frequency	Hz	0.2
D_o	O_2 diffusion capacity	L/mmHg/s	3.5×10^{-4}
D_c	CO_2 diffusion capacity	L/mmHg/s	7.08×10^{-3}
σ	O_2 solubility in blood plasma	mol/L/mmHg	1.4×10^{-6}
σ_c	CO_2 solubility in blood plasma	mol/L/mmHg	3.3×10^{-5}
T_h	Capillary hemoglobin concentration	mol/L	2×10^{-3}
K_T	Equilibrium constant in hemoglobin saturation function	L/mol	10^4
K_R	"	L/mol	3.6×10^6
L	"	–	1.712×10^8
h	Capillary H^+ ions concentration	mol/L	$10^{-7.4}$
r_2	Dehydration reaction rate	1/s	0.12
l_2	Hydration reaction rate	L/s/mol	1.64×10^5
δ	Reaction rate acceleration factor due to catalyzing enzyme	–	$10^{1.9}$
k_1	Muscle recoil rate	1/s	2
k_2	Conversion factor	m/s	1
k_p	Conversion factor	mmHg/m	2.5
K_n	Integrated phrenic activity jump	–	0.5
T_I/T_E	Inspiratory to expiratory ratio	–	0.5

of RSA using our new model for HR control (we also did this in [14], but at that stage, the model did not include autonomic HR control so RSA had to be induced artificially). Both tests are conducted by progressively reducing the parameters c_0 and S_M (representing the strength of the two autonomic limbs innervating the heart), and hence could be done experimentally by application of gradual dozes of atropine and β-blockers.

To test the hypothesis that RSA improves pulmonary gas exchange, c_0 was decreased from 1 to 0 and S_M was decreased with it to maintain the same value of mean HR. The ventilatory equivalents (V_{O_2}/V_E and V_{CO_2}/V_E) were then calculated as a function of HR variation where $V_E = \int_0^{T_R} q_{in} dt$ is the total inspired air, $V_{O_2} = \int_0^{T_R} D_o(p_{ao} - p_o)\, dt$ is the volume of O_2 taken up by the blood and $V_{CO_2} = \int_0^{T_R} D_c(p_c - p_{ac})\, dt$ is the volume of CO_2 taken out of the blood. When we kept the respiratory conditions at $T_R = 10$ s, $V_T = 1$ L ($K_n = 0.83$), $T_I = T_E$ and mean HR at 76.6 ± 0.05 bpm the improvement in gas exchange due to RSA was not significant, as has been shown previously [14]. Linear baroreflex was used for this experiment, but the non-linear B_R did not change the results qualitatively.

To test the hypothesis that RSA helps minimize the work done by the heart while keeping $\bar{p}_{ce}$, the mean arterial blood partial pressure of CO_2, constant [14], c_0 is decreased from 1 to 0 and S_M is decreased with it, but this time maintaining the same mean arterial CO_2 tension. The work done by the heart per breath is then calculated as $E = V_c^2 R_s \int_0^{T_R} \mathrm{HR}^2\, \mathrm{dt}$ (see [14]) and plotted against HR variation (Fig. 11). The results in Fig. 11 were obtained with $T_R = 10$ s, $V_T = 1$ L ($K_n = 0.83$) and $T_I = T_E$, and $\bar{p}_{ce}$ was kept at 37.11 ± 0.02 mm Hg. The energy curve has a clear minimum at about 12 bpm (just about the normal RSA magnitude in humans). The energy saving at the minimum is 2.7% compared with no RSA, very similar to the results reported by us previously [14]. It was shown in [14] that a 3% energy saving translates to saving 35 cal/h, and hence might give an evolutionary advantage. It is not directly clear from the heart rate control model of Eqs. 1,2 how the work done by the heart is influenced by RSA, however [14] provides a hydrodynamic analogy that could help explain this. Linear baroreflex is used for this experiment. The non-linear B_R does not change the results qualitatively (but the minimum does shift to an unrealistic physiological value of about ΔHR = 30 bpm, consistent with Fig. 5(c), and there is a small increase in the energy saving).

5. Discussion and conclusions

We have developed a new minimal model for the autonomic control of heart rate. The model is relatively simple compared to some of the previously-published models (see the Introduction) but we show that it can still reproduce a wide range of physiological observations and that it can be used to study the causes and benefits of RSA. The model parameters were set in Part A of the study such that the model reproduced the dependency of heart beat period on mean arterial pressure and the dependency of RSA on mean vagal tone, tidal volume and respiratory frequency. In Part B of the study we showed that the model predicts an increase in RSA amplitude under deep and slow breathing, that the phase between heart rate and lung volume is in qualitative agreement with experiments and we confirmed the hypothesis that RSA minimizes the work done by the heart while maintaining arterial CO_2.

Our model makes several new predictions:

1. That the respiratory gating of the baroreflex signal is responsible for the dependence of RSA on mean vagal tone (Fig. 3). We showed that this result is robust under changes in parameters (see Section 4.1.2).
2. That the peak in RSA amplitude when the respiratory frequency is reduced (Fig. 5) is due to the baroreflex. This result was observed only when the linear B_R was used and was shown to be true for a wide range of parameter values by analyzing the analytical solution of a simplified version of the linear case (see Section 4.1.4). Moreover, our analysis showed (see Eq.

(10)) that there is a link between the slope of $B_R(T_L)$, the sinoatrial node time response and the respiratory frequency in which RSA amplitude is maximized. There are several possible reasons for why the results using the nonlinear B_R do not agree with experiments for low values of respiratory frequency. These are discussed in Section 5.1 below.

3. That the mean HR increases linearly with increased tidal volume (assuming that the baroreflex functional form is linear, see Fig. 8).
4. That lower mean HR reduces RSA amplitude if ventilation is maintained at the same level (Fig. 9).
5. That larger inspiration-to-expiration ratios decrease the time between end of inspiration and the maximal HR reached in a single breath (Fig. 10).
6. That cardiac vagal nerve is driven with the output of the central respiratory rhythm-generating signal (A, Fig. 1(a)), which primarily sets the frequency of breathing in our model and not by the output of the ventral respiratory group (the phrenic nerve signal, R_p, Fig. 1(b)), which mainly controls the tidal volume in our model. The difference between the two driving signals is most apparent in an equivalent experiment to that of Fig. 5 where the amplitude is kept constant while the frequency of breathing is varied. The change of frequency affects the amplitude of breathing due to the integration of the signal A at the level of the ventral respiratory group (which creates the ramp seen in R_p). In order to keep the volume constant, adjustments to R_p are needed and this is done in the model by changing the parameter K_n. If R_p drives the cardiac vagal nerve these necessary adjustments in the driving signal lead to values of RSA amplitude and mean HR widely outside of the physiological range. The signal A is not affected by K_n and hence, if A drives the cardiac vagal nerve, the model output is physiologically realistic. This result does not contradict current physiological knowledge although the study of the central respiratory rhythm-generator and its influence on the cardiac vagal motor neurons is still ongoing.

5.1. Limitations of the model

In our model the neural control of heart rate is assumed to be solely mediated by the parasympathetic autonomic limb while the sympathetic signal is assumed to act on a much slower scale and is therefore only included as a constant term. This assumption may no longer hold under low respiratory frequency as the parasympathetic signal is also modulated more slowly by the central respiratory signal and the mechanical stretch receptors. Nevertheless, the linear model of the baroreflex gave good agreement with experimental results over this low frequency range, just as it has done for all the other experiments we used to validate the model (see also end of Section 4.2.7). This suggests that there are other mechanisms that act to keep the mean arterial pressure in the linear range and the sympathetic signal could be one of them. In addition, the shape of the B_R function shown in Fig. 2 might change for different breathing patterns (but there is no experimental data to validate this).

In our model the baroreflex only responds to changes in mean arterial pressure (MAP) and furthermore, we assumed that the stroke volume (V_c) and the systemic vascular resistance (R_S) are constants. The absence of blood-pressure oscillations over a heart-beat period makes it impossible for us to study the effects of systolic/diastolic pressure fluctuations on RSA. Whether this limitation affects our results significantly remains to be studied by comparing our results to more detailed cardio-respiratory models.

We chose to ignore the effect of peripheral chemoreceptors on HR [72]. Peripheral chemoreceptors are mostly sensitive to O_2 and affect both the respiratory and cardiovascular systems. The primary effect of stimulating the carotid chemoreceptors with either hypoxia or hypercapnia on HR is bradycardia (a decrease in HR) while stimulation of the aortic chemoreceptors results in tachycardia (an increase in HR). Moreover, carotid chemostimulation leads to concurrent primary vasoconstriction (an increase in vascular resistance triggered by sympathetic activation) while local hypoxia causes vasodilation. Finally, if ventilation is allowed to increase in response to carotid chemostimulation, mechanical feedback from the lungs will act to accelerate the HR. Under the same conditions, hyperventilation will lead to hypocapnia, also causing a secondary cardiac acceleration. In humans, one almost always observes tachycardia – in other words, the primary cardiac chemoreflex is masked by the secondary effects. We therefore decided to exclude the cardiac chemoreflex from the model. On the other hand, we have previously incorporated ventilatory control [68] into the model, and although this aspect is "switched off" for the present study, by enabling ventilatory control we should obtain the observed tachycardia due to mechanical feedback, as found experimentally in spontaneously breathing man.

Taking the respiratory system in open loop (i.e. "switched off" control) enabled us to mimic experiments where subjects were told to breathe in a particular way (commonly used to study RSA). However, it prevented us from exploring the coupling between the heart and the lungs under spontaneous breathing. This coupling, as well as the effect of chemical control on HR, will be the subject of future study.

Acknowledgment

This work was partly supported by NIH Grant R01 NS069220. We would like to thank the anonymous reviewers for their useful suggestions.

Appendix A. Lung model

Here we list the equations of the lung model for convenience. See [69,68] for a full derivation and discussion of the model dynamics.

The model consists of seven differential equations that have to be numerically integrated:

$$\frac{dP_A}{dt} = \frac{P_m E}{P_A} Q_A + \frac{dP_L}{dt}, \tag{A.1}$$

$$\frac{df_o}{dt} = \frac{1}{V_A}\{D_o(p_o - p_{ao}) + q_i(f_{oi} - f_o) - f_o[D_c(p_c - p_{ac}) + D_o(p_o - p_{ao})]\}, \tag{A.2}$$

$$\frac{df_c}{dt} = \frac{1}{V_A}\{D_c(p_c - p_{ac}) + q_i(f_{ci} - f_c) - f_c[D_o(p_o - p_{ao}) + D_c(p_c - p_{ac})]\}, \tag{A.3}$$

$$\frac{dp_o}{dt} = \frac{D_o}{C_u \sigma V_c}\left(1 + \frac{4T_h}{\sigma}\frac{dS}{dp_o}\right)^{-1}[f_o(P_A - p_w) - p_o], \tag{A.4}$$

$$\frac{dp_c}{dt} = \frac{D_c}{C_u \sigma_c V_c}(p_{ac} - p_c) + \frac{\delta \ell_2}{\sigma_c} hz - \delta r_2 p_c, \tag{A.5}$$

$$\frac{dz}{dt} = \delta r_2 \sigma_c p_c - \delta \ell_2 hz, \tag{A.6}$$

$$\frac{dx_m}{dt} = -k_1 x_m + k_2 R_p. \tag{A.7}$$

The variables being solved for are: P_A – the total alveolar pressure, f_o and f_c – the alveolar fractional (dry) concentrations of oxygen and

carbon dioxide respectively, p_o, p_c – the arterial partial pressures of O_2 and CO_2 respectively, z – the arterial concentration of HCO_3^- and x_m – the diaphragm muscle displacement. The values of p_o, p_c and z are initialized every heart beat as the model is integrated forward in time. The "reset" values were taken as $p_o = 40$ mm Hg, $p_c = 46$ mm Hg and $z = p_c(0)\sigma_c r_2/(h\ell_2)$. The values of p_o and p_c just before the "reset" represent the blood partial pressures of O_2 and CO_2 respectively when blood leaves the lungs (denoted by p_{oe} and p_{ce} respectively). The other variables appearing in the differential equations are:

$$Q_A = q + D_c(p_c - p_{ac}) + D_o(p_o - p_{ao}), \tag{A.8}$$

$$q = \frac{P_m - P_A}{R}, \tag{A.9}$$

$$P_L(t) = P_m - P_{L0} - k_p x_m, \tag{A.10}$$

$$V_A = \frac{P_A - P_L}{E}, \tag{A.11}$$

$$p_{ao} = f_o(P_A - p_w), \tag{A.12}$$

$$p_{ac} = f_c(P_A - p_w), \tag{A.13}$$

$$S(p_o) = \frac{LK_T\sigma p_o(1 + K_T\sigma p_o)^3 + K_R\sigma p_o(1 + K_R\sigma p_o)^3}{L(1 + K_T\sigma p_o)^4 + (1 + K_R\sigma p_o)^4}, \tag{A.14}$$

where Q_A is the net flux of gas into the lungs, q is the air-flow, q_i (appears in Eqs. (A.2) and (A.3)) is the air-flow during inspiration ($q_i = 0$ during expiration), P_L is the pleural pressure, V_A is the alveolar volume, p_{ao} and p_{ac} are the alveolar partial pressures of O_2 and CO_2 receptively and $S(p_o)$ is the Hemoglobin saturation function. f_{oi} and f_{ci} (appear in Eqs. (A.2) and (A.3)) are the inspired concentrations of oxygen and carbon dioxide, respectively and are calculated by the following prescription (replace 'o' by 'c' subscripts to get the rules for f_{ci}):

$$\begin{aligned} &f_{oi} = f_{om}; \quad V_i > V_D \quad \text{and} \quad (P_m - P_A) > 0, \\ &f_{oi} = f_{od}; \quad V_i \leqslant V_D \quad \text{and} \quad (P_m - P_A) > 0, \\ &f_{oi} = f_o; \quad (P_m - P_A) \leqslant 0, \end{aligned} \tag{A.15}$$

where V_D is the dead space volume, V_i is the inspired volume of the lungs and is calculated by integrating the airflow during inspiration using the trapezoidal rule, f_{om} is the concentration of oxygen in the mouth, and f_{od} is the concentration of oxygen in the alveolar dead space (calculated as the lung concentration of oxygen at the end of expiration).

The activity of the pre-Botzinger complex is modeled as a square wave (see Fig. 1 (a)):

$$A = \begin{cases} A_t & \text{if} \quad \text{mod}(t, T_R) \leqslant T_I, \\ A_b & \text{if} \quad T_I < \text{mod}(t, T_R) \leqslant T_E, \end{cases} \tag{A.16}$$

In all of our simulations $A_t = 0.43$ and $A_b = 0.28$. The phrenic nerve signal R_p (see Eq. (A.7) and Fig. 1(b)) is calculated from A in the following way:

$$R_p(t) = \begin{cases} K_n & \text{if } A(t) \geqslant T_{r1} \quad \text{and} \quad R_p(t - \Delta t) <= 0.001 \\ I_p & \text{if } A(t) \geqslant T_{r1} \quad \text{and} \quad R_p(t - \Delta t) > 0.001 \\ 0 & \text{if } A(t) < T_{r1} \end{cases} \tag{A.17}$$

where $I_p = [A(t) - I_l R_p(t - \Delta t)]\Delta t + R_p(t - \Delta t)$. $I_l = 0.1$ in Fig. 1(b). Note that this formula is equivalent to the one given in Eq. (5) of [68] when Δt is fixed. But while in [68] I_l depends on Δt there is no such dependency in the formula we use here. In all of our simulations $T_{r1} = 0.35$.

The meaning and values of all the other parameters in this model are given in Table 4. These parameters are typical for humans (i.e. represent an average subject) and are used as the default if an explicit value is not mentioned when specific results are presented. All values are taken from [68].

References

[1] K.M. Spyer, Central nervous integration of cardiovascular control, J. Exp. Biol. 100 (OCT) (1982) 109–128.
[2] L. Sherwood, Human Physiology: From Cells to Systems, second ed., West Pub. Co., 1993.
[3] T.D. Bradley, J.S. Floras (Eds.), Sleep Apnea – Implications in Cardiovascular and Cerebrovascular Disease, Marcel Dekker Inc., New York, 2000.
[4] F. Yasuma, J. Hayano, Respiratory sinus arrhythmia – why does the heartbeat synchronize with respiratory rhythm?, Chest 125 (2) (2004) 683–690
[5] P. Grossman, E.W. Taylor, Toward understanding respiratory sinus arrhythmia: relations to cardiac vagal tone, evolution and biobehavioral functions, Biol. Psychol. 74 (2) (2007) 263–285.
[6] D.L. Eckberg, Point: counterpoint: respiratory sinus arrhythmia is due to a central mechanism vs. respiratory sinus arrhythmia is due to the baroreflex mechanism, J. Appl. Physiol. 106 (5) (2009) 1740–1742.
[7] J.M. Karemaker, Counterpoint: respiratory sinus arrhythmia is due to the baroreflex mechanism, J. Appl. Physiol. 106 (5) (2009) 1742–1743.
[8] C. Julien, Comments on point: counterpoint: respiratory sinus arrhythmia is due to a central mechanism vs. respiratory sinus arrhythmia is due to the baroreflex mechanism, J. Appl. Physiol. 106 (5) (2009) 1745–1749.
[9] J.M. Karemaker, Last word on point: counterpoint: respiratory sinus arrhythmia is due to a central mechanism vs. respiratory sinus arrhythmia is due to the baroreflex mechanism, J. Appl. Physiol. 106 (5) (2009) 1750.
[10] P.D. Larsen, Y.C. Tzeng, P.Y.W. Sin, D.C. Galletly, Respiratory sinus arrhythmia in conscious humans during spontaneous respiration, Resp. Physiol. Neurobiol. 174 (1–2) (2010) 111–118.
[11] M.P. Gilbey, D. Jordan, D.W. Richter, K.M. Spyer, Synaptic mechanisms involved in the inspiratory modulation of vagal cardio-inhibitory neurones in the cat, J. Physiol. 356 (1984) 65–78.
[12] K.M. Spyer, Central nervous mechanisms responsible for cardio-respiratory homeostasis, Adv. Exp. Med. Biol. 381 (1995) 73–79.
[13] J. Hayano, F. Yasuma, A. Okada, S. Mukai, T. Fujinami, Respiratory sinus arrhythmia – phenomenon improving pulmonary gas exchange and circulatory efficiency, Circulation 94 (4) (1996) 842–847.
[14] A. Ben-Tal, S.S. Shamailov, J.F.R. Paton, Evaluating the physiological significance of respiratory sinus arrhythmia: looking beyond ventilation–perfusion efficiency, J. Physiol.-Lond. 590 (8) (2012) 1989–2008.
[15] A. Rosenblueth, F.A. Simeone, The interrelations of vagal and accelerator effects on the cardiac rate, Am. J. Physiol. 110 (1) (1934) 42–55.
[16] G.F. Chess, F.R. Calaresu, Mathematical-model of vagus-heart period system in cat, IEEE Trans. Biomed. Eng. BM21 (1) (1974) 21–27.
[17] H.R. Warner, A. Cox, A mathematical model of heart rate control by sympathetic and vagus efferent information, J. Appl. Physiol. 17 (2) (1962) 349–355.
[18] P.G. Katona, P.J. Martin, F. Jih, Neural control of heart-rate – conciliation of models, IEEE Trans. Biomed. Eng. 23 (2) (1976) 164–166.
[19] A. Mokrane, R. Nadeau, Dynamics of heart rate response to sympathetic nerve stimulation, Am. J. Physiol.-Heart Circ. Physiol. 275 (3) (1998) H995–H1001.
[20] H.R. Warner, R.O. Russell, Effect of combined sympathetic and vagal stimulation on heart rate in dog, Circ. Res. 24 (4) (1969) 567–573.
[21] J.J. Zebrowski, K. Grudzinski, T. Buchner, P. Kuklik, J. Gac, G. Gielerak, P. Sanders, R. Baranowski, Nonlinear oscillator model reproducing various phenomena in the dynamics of the conduction system of the heart, Chaos 17 (1) (2007) 015121.
[22] S. Cavalcanti, Arterial baroreflex influence on heart rate variability: a mathematical model-based analysis, Med. Biol. Eng. Comput. 38 (2) (2000) 189–197.
[23] K. Kotani, K. Takamasu, Y. Ashkenazy, H.E. Stanley, Y. Yamamoto, Model for cardiorespiratory synchronization in humans, Phys. Rev. E 65 (5) (2002) 051923.
[24] R.W. Deboer, J.M. Karemaker, J. Strackee, Hemodynamic fluctuations and baroreflex sensitivity in humans – a beat-to-beat model, Am. J. Physiol. 253 (3) (1987) H680–H689.
[25] H. Seidel, H. Herzel, Bifurcations in a nonlinear model of the baroreceptor-cardiac reflex, Physica D 115 (1–2) (1998) 145–160.
[26] J.B. Madwed, P. Albrecht, R.G. Mark, R.J. Cohen, Low-frequency oscillations in arterial-pressure and heart-rate – a simple computer-model, Am. J. Physiol. 256 (6) (1989) 1489–1496.
[27] M. Ursino, E. Magosso, Role of short-term cardiovascular regulation in heart period variability: a modeling study, Am. J. Physiol.-Heart Circ. Physiol. 284 (4) (2003) H1479–H1493.
[28] K. Lu, J.W. Clark, F.H. Ghorbel, D.L. Ware, J.B. Zwischenberger, A. Bidani, Whole-body gas exchange in human predicted by a cardiopulmonary model, Int. J. Cardiovasc. Eng. 3 (1) (2003) 1–19.
[29] L. Cheng, O. Ivanova, H.-H. Fan, M.C.K. Khoo, An integrative model of respiratory and cardiovascular control in sleep-disordered breathing, Resp. Physiol. Neurobiol. 174 (1–2) (2010) 4–28.

[30] K. Lu, J.W. Clark, F.H. Ghorbel, D.L. Ware, A. Bidani, A human cardiopulmonary system model applied to the analysis of the valsalva maneuver, Am. J. Physiol.-Heart Circ. Physiol. 281 (6) (2001) H2661–H2679.
[31] M. Barbi, A. Di Garbo, R. Balocchi, Improved integrate-and-fire model for rsa, Math. Biosci. Eng. 4 (4) (2007) 609–616.
[32] B.F. Womack, Analysis of respiratory sinus arrhythmia using spectral analysis and digital filtering, IEEE Trans. Biomed. Eng. BM18 (6) (1971) 399–409.
[33] M. Clynes, Respiratory sinus arrhythmia – laws derived from computer simulation, J. Appl. Physiol. 15 (5) (1960) 863–874.
[34] Y. Shiogai, A. Stefanovska, P.V.E. McClintock, Nonlinear dynamics of cardiovascular ageing, Phys. Rep.-Rev. Sect. Phys. Lett. 488 (2–3) (2010) 51–110.
[35] A. Ben-Tal, Computational models for the study of heart-lung interactions in mammals, Wiley Interdiscipl. Rev.-Syst. Biol. Med. 4 (2) (2012) 163–170.
[36] F. Dexter, Y. Rudy, M.N. Levy, E.N. Bruce, Mathematical-model of cellular basis for the respiratory sinus arrhythmia, J. Theor. Biol. 150 (2) (1991) 157–173.
[37] R.M. Negoescu, I.E. Csiki, Model of respiratory sinus arrhythmia in man, Med. Biol. Eng. Comput. 27 (3) (1989) 260–268.
[38] E.K. Potter, Inspiratory inhibition of vagal responses to baroreceptor and chemoreceptor stimuli in the dog, J. Physiol. 316 (1981) 177–190.
[39] A.L. Davis, D.L. McColskey, E.K. Potter, Respiratory modulation of baroreceptor and chemoreceptor reflexes affecting heart rate through the sympathetic nervous system, J. Physiol. 272 (3) (1977) 691–703.
[40] Engauge Digitizer – Digitizing Software. <http://sourceforge.net/projects/digitizer/files/>.
[41] J.M. Fritschyelle, J.B. Charles, M.M. Jones, L.A. Beightol, D.L. Eckberg, Spaceflight alters autonomic regulation of arterial-pressure in humans, J. Appl. Physiol. 77 (4) (1994) 1776–1783.
[42] C.H. Davos, L.C. Davies, M. Piepoli, The effect of baroreceptor activity on cardiovascular regulation, Hellenic J. Cardiol. 43 (2002) 145–155.
[43] F. Lador, E. Tam, M.A. Kenfack, M. Cautero, C. Moia, D.R. Morel, C. Capelli, G. Ferretti, Phase I dynamics of cardiac output, systemic O_2 delivery, and lung O_2 uptake at exercise onset in men in acute normobaric hypoxia, Am. J. Physiol.-Reg. Integr. Comp. Physiol. 295 (2) (2008) R624–R632.
[44] P.I. Korner, M.J. West, J. Shaw, J.B. Uther, Steady-state properties of baroreceptor heart rate reflex in essential hypertension in man, Clin. Exp. Pharmacol. Physiol. 1 (1) (1974) 65–76.
[45] J. Tank, A. Diedrich, E. Szczech, F.C. Luft, J. Jordan, Baroreflex regulation of heart rate and sympathetic vasomotor tone in women and men, Hypertension 45 (6) (2005) 1159–1164.
[46] G.V. Anrep, W. Pascual, R. Rossler, Respiratory variations of the heart rate i – the reflex mechanism of the respiratory arrhythmia, Proc. R. Soc. London Ser. B–Biol. Sci. 119 (813) (1936) 191–217.
[47] P.G. Katona, F. Jih, Respiratory sinus arrhythmia – noninvasive measure of parasympathetic cardiac control, J. Appl. Physiol. 39 (5) (1975) 801–805.
[48] M. Kollai, G. Mizsei, Respiratory sinus arrhythmia is a limited measure of cardiac parasympathetic control in man, J. Physiol.-Lond. 424 (1990) 329–342.
[49] H. Kobayashi, Normalization of respiratory sinus arrhythmia by factoring in tidal volume, Appl. Human Sci. 17 (5) (1998) 207–213.
[50] K.P. Ohagan, L.B. Bell, P.S. Clifford, Effects of pulmonary denervation on renal sympathetic and heart-rate responses to hypoxia, Am. J. Physiol.-Reg. Integr. Comp. Physiol. 269 (4) (1995) R923–R929.
[51] P.M. Simon, B.H. Taha, J.A. Dempsey, J.B. Skatrud, C. Iber, Role of vagal feedback from the lung in hypoxic-induced tachycardia in humans, J. Appl. Physiol. 78 (4) (1995) 1522–1530.
[52] A. Berakis, T.J. Williams, M.T. Naughton, J.H. Martin, M. Muhlmann, H. Krum, Altered sympathetic and parasympathetic activity in lung transplantation patients at rest and following autonomic perturbation, Chest 122 (4) (2002) 1192–1199.
[53] N.J. Morgan-hughes, P.A. Corris, M.D. Healey, J.H. Dark, J.M. McComb, Cardiovascular and respiratory effects of adenosine in humans after pulmonary denervation, J. Appl. Physiol. 76 (2) (1994) 756–759.
[54] G.F. Chess, F.R. Calaresu, Frequency response model of vagal control of heart rate in cat, Am. J. Physiol. 220 (2) (1971) 554–557.
[55] J.A. Hirsch, B. Bishop, Respiratory sinus arrhythmia in humans – how breathing pattern modulates heart-rate, Am. J. Physiol. 241 (4) (1981) H620–H629.
[56] H.S. Song, P.M. Lehrer, The effects of specific respiratory rates on heart rate and heart rate variability, Appl. Psychophys. Biof. 28 (1) (2003) 13–23.
[57] A. Angelone, N.A. Coulter, Respiratory sinus arrhythmia: a frequency dependent phenomenon, J. Appl. Physiol. 19 (3) (1964) 479–482.
[58] P.G. Katona, J.W. Poitras, G.O. Barnett, B.S. Terry, Cardiac vagal efferent activity and heart period in carotid sinus reflex, Am. J. Physiol. 218 (4) (1970) 1030–1037.
[59] N.D. Giardino, R.W. Glenny, S. Borson, L. Chan, Respiratory sinus arrhythmia is associated with efficiency of pulmonary gas exchange in healthy humans, Am. J. Physiol.-Heart Circ. Physiol. 284 (5) (2003) H1585–H1591.
[60] H.V. Sparks, T.W. Rooke, ebrary Inc, University of Minnesota Press, Essentials of cardiovascular physiology, 1987.
[61] A.E. Simms, J.F.R. Paton, A.E. Pickering, Hierarchical recruitment of the sympathetic and parasympathetic limbs of the baroreflex in normotensive and spontaneously hypertensive rats, J. Physiol.-Lond. 579 (2) (2007) 473–486.
[62] D.L. Eckberg, C.R. Orshan, Respiratory and baroreceptor reflex interactions in man, J. Clin. Invest. 59 (5) (1977) 780–785.
[63] S.C. Gandevia, D.I. McCloskey, E.K. Potter, Inhibition of baroreceptor and chemoreceptor reflexes on heart-rate by afferents from lungs, J. Physiol.-Lond. 276 (MAR) (1978) 369–381.
[64] O.U. Lopes, J.F. Palmer, Proposed respiratory gating mechanism for cardiac slowing, Nature 264 (5585) (1976) 454–456.
[65] A.L. Davis, D.I. McCloskey, E.K. Potter, Respiratory modulation of baroreceptor and chemoreceptor reflexes affecting heart-rate through sympathetic nervous-system, J. Physiol.-Lond. 272 (3) (1977) 691–703.
[66] B.T. Haymet, D.I. McCloskey, Baroreceptor and chemoreceptor influences on heart-rate during respiratory cycle in dog, J. Physiol.-Lond. 245 (3) (1975) 699–712.
[67] G.V. Anrep, W. Pascual, R. Rossler, Respiratory variations of the heart rate ii – the central mechanism of the respiratory arrhythmia and the inter-relations between the central and the reflex mechanisms, Proc. R. Soc. London Ser. B–Biol. Sci. 119 (813) (1936) 218–232.
[68] A. Ben-Tal, J.C. Smith, A model for control of breathing in mammals: coupling neural dynamics to peripheral gas exchange and transport, J. Theor. Biol. 251 (3) (2008) 480–497.
[69] A. Ben-Tal, Simplified models for gas exchange in the human lungs, J. Theor. Biol. 238 (2) (2006) 474–495.
[70] S. Ogoh, J. Fisher, E. Dawson, M. White, N. Secher, P. Raven, Autonomic nervous system influence on arterial baroreflex control of heart rate during exercise in humans, J. Physiol. 566 (Pt 2) (2005) 599–611.
[71] Y.C. Tzeng, P.D. Larsen, D.C. Galletly, Effects of hypercapnia and hypoxemia on respiratory sinus arrhythmia in conscious humans during spontaneous respiration, Am. J. Physiol.-Heart Circ. Physiol. 292 (5) (2007) H2397–H2407.
[72] J.H. Comroe, Physiology of Respiration: An Introductory Text, second ed., Year Book Medical Publishers, 1977.